INTRODUCTION OF PRECISELY CONTROLLED MICROSTRUCTURAL DEFECTS INTO SRF CAVITY NIOBIUM SHEETS AND THEIR IMPACT ON LOCAL SUPERCONDUCTING PROPERTIES*

M. Wang, T.R. Bieler, D. Kang, Michigan State University, East Lansing, MI 48824, USA
C.C. Compton, Facility for Rare Isotope Beams, East Lansing, MI 48824, USA
D. C. Larbalestier, P. J. Lee, A. A. Polyanskii, Z. H. Sung, Applied Superconductivity Center, National High Magnetic Field Laboratory, Tallahassee, FL 32310, USA

Abstract

When SRF (superconducting radio frequency) cavity half cells are formed from niobium sheets, the metallurgical processing introduces microstructural defects such as dislocations and low-angle grain boundaries that may degrade cavity performance. And the density and distribution of these defects may vary with the prior processing of the sheet. To build and understand the relationship between magnetic flux behavior and microstructural defects in SRF niobium we have strategically strained tensile samples cut from an SRF niobium sheet to produce specific types of microstructural defects that could then be examined for their impact on local weakness to magnetic flux penetration using magneto-optical (MO) imaging. Laue X-ray and electron backscatter diffraction (also known as orientation imaging microscopy™, EBSD or OIM) crystallographic analyses of large grain ingot slices were used to characterize microstructural defects in order to enable eventual prediction of which grain and sample orientations will produce defects due to tensile deformation. Grain orientations were chosen to favor specific slip systems, which generate dislocations with particular angles with respect to the sample surface. The generated defect structures were characterized using OIM and transmission electron microscopy (TEM). MO imaging showed, for the first time, preferential flux penetration associated with local regions with high dislocation density.

INTRODUCTION

High purity niobium, with the highest critical temperature of the elemental superconductors, is widely used for superconducting radio frequency (SRF) cavities [1]. As particle accelerators have important applications in several fields, increasing the accelerating electric field and quality factor of cavities have always been pursued. The limit value of maximum accelerating field has been reached, but not in a reproducible way [2, 3]. This variability of cavity performance needs to be minimized to reduce the cost of future instruments.

From the view point of materials science, microstructural evolution during processes, such as rolling, drawing, welding and heat treatment, can generate many possible defects that could account for the some of the inconsistencies in cavity performance. Hence, it is desirable to understand and ultimately control the amount and kinds of microstructural defects in niobium that can interact with the magnetic field in the cavity and degrade cavity performance. The maximum magnetic field occurs in the equator area of elliptical niobium cavities, where "hot spots" (local overheated areas) are often observed during operation of the cavities. The magnetic field is caused by the high superconducting currents going around the equator region along the innermost layer of material (10's of nanometers). Evidence has been found that these "hot spots" originate from trapped magnetic flux within niobium [4]. Local thermal gradients can displace the trapped flux and weaken the "hot spots" [4]. Pinning centers that tend to trap magnetic flux include dislocations and low angle grain boundaries (LAGB) that are introduced during the fabrication of niobium cavities. These defects with magnetic flux pinned around them could lead to the loss of superconductivity in local areas, where the density of superconducting electrons is close to zero [5]. This perturbation for the superconducting currents due to grain boundaries has been observed using cryogenic magneto-optical (MO) imaging [6].

Not only does flux trapping limit the accelerating field, it also generates extra heat that has to be transferred out through liquid helium coolant which needs extra energy to keep it at a low temperature (<9.3K). Although magnetic flux behavior due to microstructural defects is believed to cause problems, few researchers have investigated the mechanism. Flux penetration has been observed when grain boundaries are perpendicular to the surface of the MO sample and parallel to the magnetic field [6]. To discover the mechanisms, it is necessary to investigate correlations between microstructural defects and magnetic flux behavior within niobium.

In this work, high purity SRF niobium tensile samples were strategically deformed in a way similar to that of typical cavity forming processes to introduce dislocations that have specific angles with respect to the sample surface. This is based on the assumption that screw dislocations dominate the microstructure, as commonly observed in BCC metals [7]. The cryogenic MO imaging

*Research supported by DOE/OHEP (contract number DE-FG02-09ER41638 at MSU and DE-SC0009960 at FSU) and the State of Florida.

technique was then used to directly observe the magnetic flux behavior in the deformed samples.

SAMPLE PREPARATION

Niobium Disk

A high purity niobium disk with a diameter of 270 mm and a thickness of 3 mm was provided by Tokyo Denkai. This large grain disk had been sliced from a multiple electron beam melting (EBM) [1] processed ingot using electrical discharge machining (EDM), as shown in Fig. 1.

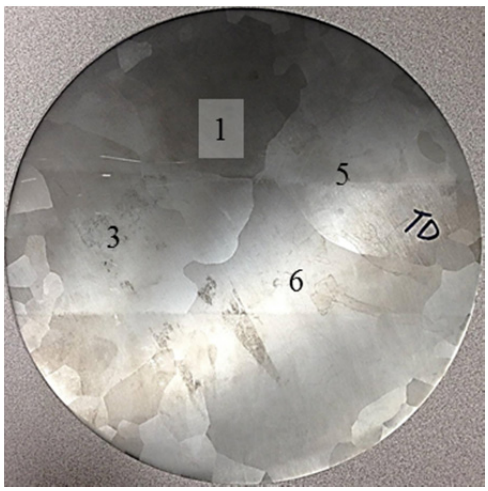

Figure 1: High purity niobium disk sliced from an ingot with four large grains numbered.

Laue X-ray Diffraction and Grain Orientation

The four largest grains (marked as grain 1, 3, 5, and 6 in Fig. 1) were chosen, so that there was enough space to extract tensile samples from the disk. Before sample extraction, Laue X-ray diffraction was carried out on the disk to obtain diffraction patterns for each grain, which were then indexed using OrientExpress software. A MATLAB code was used to convert the index results into Bunge Euler angles, which were then used to generate an orientation map of the crystals, as shown in Fig. 2 and Table 1. The colors in the orientation map in Fig. 2 represent the crystal direction in the normal direction, and the prisms show the actual crystal orientations.

The general strategy for sample extraction is to choose tensile directions in tensile samples that will favor specific slip systems. Following prior work, orientations that lead to dislocations and grain boundaries being parallel or perpendicular to the sample surface were chosen for MO imaging [6].

Schmid Factor Calculation and Tensile Axes

The Schmid factor is a definition used in materials science to describe the likelihood of activating a slip system. For body-centered cubic (BCC) crystals, including niobium, the value of Schmid factor is between 0 and 0.5, with 0.5 representing the softest orientation, meaning that the resolved shear stress on the slip system is as high as it can be. Using this information, the tensile direction was carefully chosen to activate specific dislocation slip systems in niobium for MO imaging.

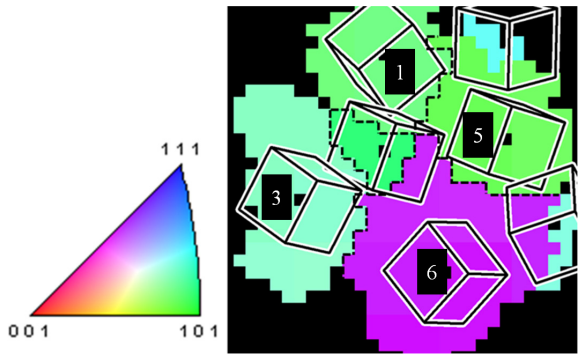

Figure 2: Normal direction orientation map of niobium disk, with colors representing crystal directions in the normal direction.

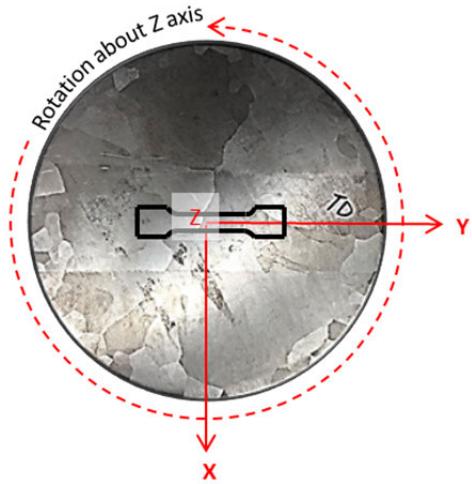

Figure 3: Schematic of rotation of niobium disk in the MATLAB code which calculates Schmid factors of all slip systems for each degree of rotation over 360°.

Table 1: Bunge Euler Angles for the Four Chosen Grains on Niobium Disk

Grain #	φ_1	Φ	φ_2
Grain 1	317	141	190
Grain 3	167	141	108
Grain 5	337	141	175
Grain 6	178	147	135

A MATLAB code was developed in our group to compute Schmid factors based on a given grain orientation [8]. This code calculates the Schmid factors of all slip systems in BCC crystals over a 360° rotation of the tensile axis about the sample normal direction (Z) around the perimeter of the slice of the niobium disk surface as shown in Fig. 3.

Slip on {110} and {112} planes in <111> directions are commonly observed in BCC crystals, and each of these 24 slip systems is shown systematically with colors (blue for {112} and green for {110} planes) and types of lines (same kind of line for systems with the same <111> direction) (Fig. 4). The example of Schmid factor calculation shown in Fig. 4 is based on the orientation of

ISBN 978-3-95450-178-6

grain 5. The solid red line marks the original orientation of grain 5 before rotation, while the dashed red line shows the orientation that maximizes the shear stress on the $(2\bar{1}1)[\bar{1}\bar{1}1]$ system (marked with red ellipse). This requires only a 10° rotation for dislocations with the $[\bar{1}\bar{1}1]$ Burgers vector, which is nearly parallel to the sample surface, to be generated during deformation. A similar calculation and orientation choosing strategy was applied to other three grains. Figure 5 shows the layout of tensile samples in the niobium disk with the required angles of rotations to highly favor particular slip systems shown in Fig. 6 such that the Burgers vectors were nearly parallel to the surface. EDM was then used to extract these tensile samples from the disk.

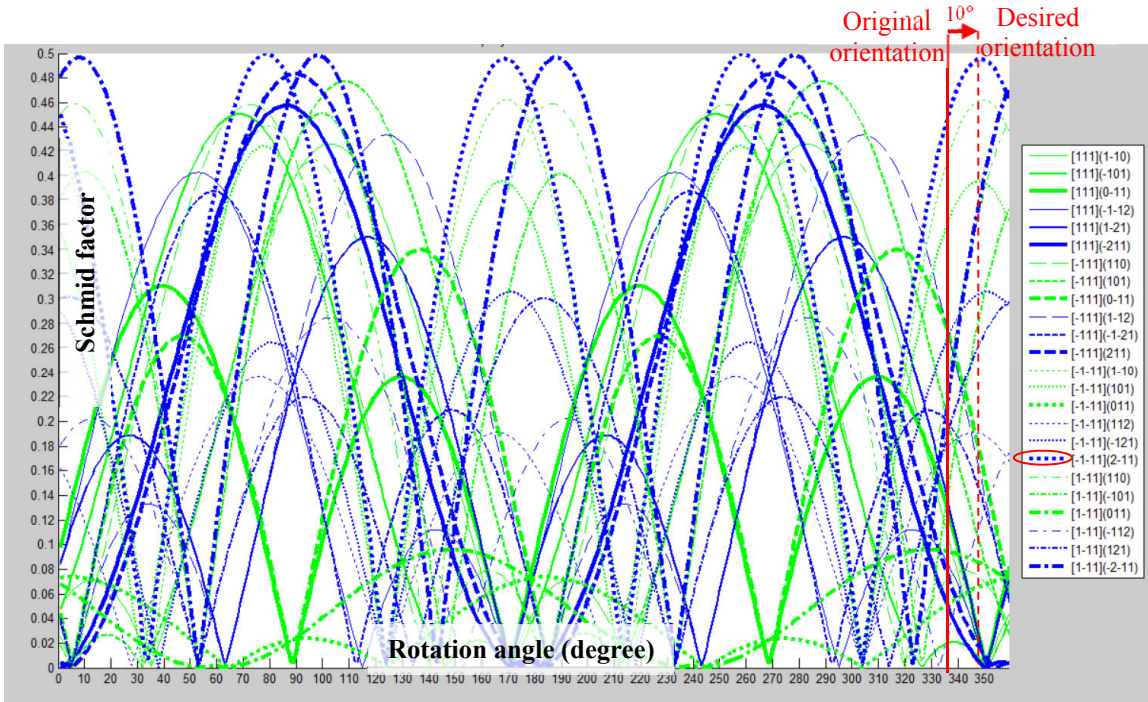

Figure 4: Absolute value of Schmid factor calculation for all slip systems over 360°, with red solid line representing the original orientation and red dashed line the desired orientation to favor $(2\bar{1}1)[\bar{1}\bar{1}1]$ slip system in grain 5.

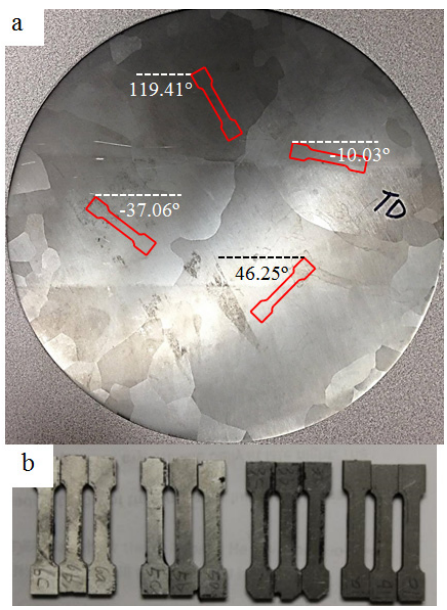

Figure 5: (a) Layout of tensile samples in each grain with rotations indicated; (b) Three identical tensile samples were extracted for each grain.

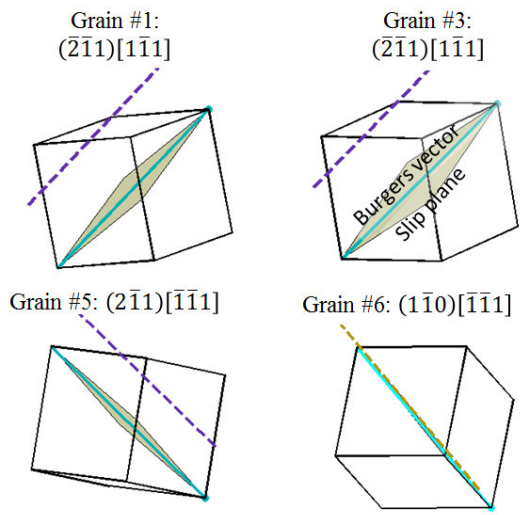

Figure 6: The most favored slip systems in four grains predicted by MATLAB code. Angles between <111> Burgers vectors (Blue-green line) and the sample surface are 0.6°, 2.9°, 2.9° and 0.12° for grain 1, 3, 5 and 6 respectively.

5% Deformation and Extraction of MO Samples

An INSTRON materials testing system was used to deform the tensile samples to 5% strain. Deformed tensile samples were further cut to obtain small pieces (MO samples) with suitable size (3x3x1.5 mm) for MO imaging, making tilted cuts to make dislocation Burgers vectors parallel or perpendicular to the section surface (screw dislocation line directions are parallel to the Burgers vector, and edge dislocation line directions are perpendicular to the Burgers vector and in the slip plane). Four MO samples were extracted from each deformed tensile sample. Two of them have screw dislocations in the section (slip) plane, while the dislocation lines are out of the section plane for the other two (Fig. 7).

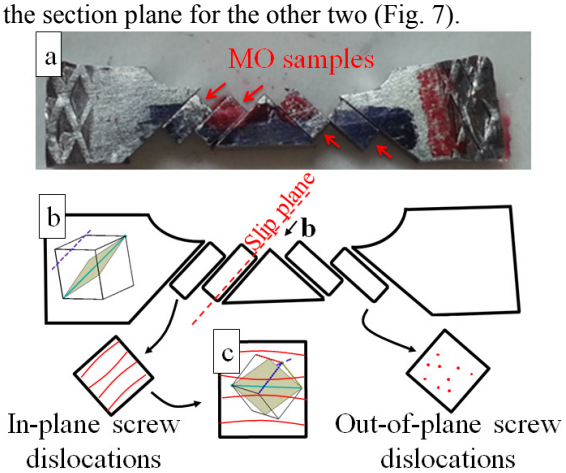

Figure 7: (a) Four small pieces (indicated by red arrows) extracted from one deformed tensile sample; (b) Screw dislocation (red lines and dots) orientation with respect to the section plane; (c) Crystal orientation from extracted MO sample perspective.

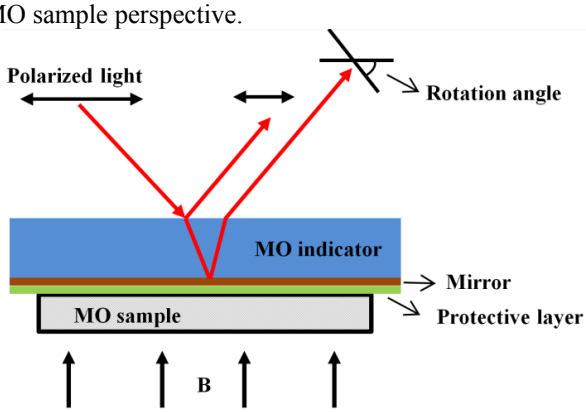

Figure 8: Schematic of MO imaging technique.

CRYOGENIC MAGNETO-OPTICAL IMAGING

MO imaging can visualize both local and global magnetic flux behavior and, as a result, the existence of defects in superconductors at temperatures below the critical temperature ($T_C = 9.3K$), [6, 9]. The basic principle behind this technique is the Farraday effect: light polarization can be rotated by a magnetic field [9-11], as shown in Fig. 8. The rotation angle of light polarization can be expressed as:

$$\text{Rotation angle} = dVB \quad (1)$$

where d is the distance the light goes through in the MO indicator, V is the Verdet constant for the material and B the applied magnetic field in the direction of the light propagation. Therefore, magnetic flux that penetrates into the MO sample can be related to the rotation of light polarization, and hence, visualized.

RESULTS AND DISCUSSION

View Point of MO Imaging

Magnetic fields were applied to the MO samples as described in Fig. 9. The magnetic field in case 1 is perpendicular to the original tensile sample surface (rectangle), while in case 2 the field is perpendicular to the section plane (square). MO images were taken along the same directions as the applied magnetic field from one side of the MO sample.

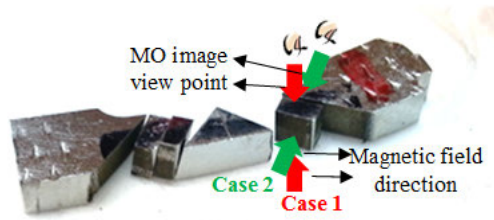

Figure 9: View point of MO imaging with both case 1 and case 2 magnetic fields.

MO Images

In MO images, image intensity is proportional to the density of magnetic flux. Due to space limitations, only results of case 2 are presented. Figure 10 shows the MO contrast of a sample in a magnetic field that is perpendicular to the sample surface (the plane of page).

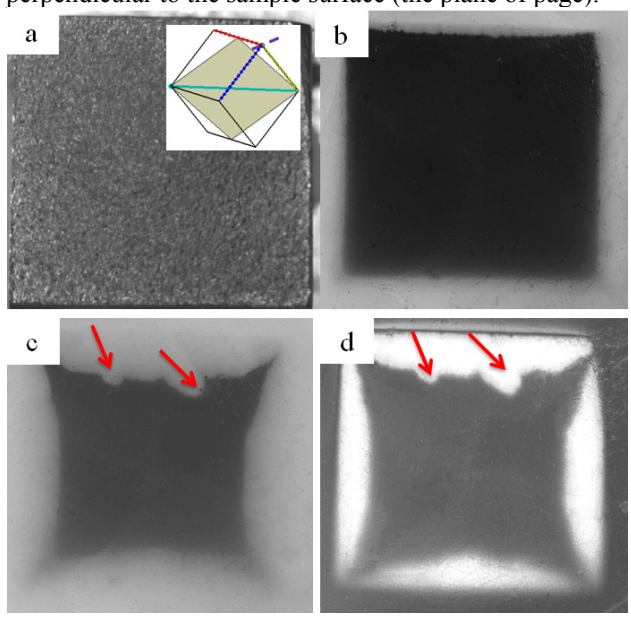

Figure 10: (a) Optical sample surface (3.1x3.07 mm) and $(\bar{2}\bar{1}1)[1\bar{1}1]$ slip system in a unit cell (on shaded plane);

ISBN 978-3-95450-178-6

(b) MO image taken in zero-field-cooled (ZFC) condition with T = 8.2K and magnetic field H = 20mT; (c) MO image, ZFC, T = 8.2K, H = 40mT; (d) MO image of trapped magnetic flux at T = 8.2K, zero magnetic field (reduced from H = 40mT).

Figure 10 (a) shows a conventional light microscope image of the surface with a unit cell indicating the orientation and most favored slip system of this sample. The blue-green line is the Burgers vector, as well as screw dislocation line direction. (b), (c) and (d) show the change of MO contrast with the increase of applied magnetic field. Clear contrast of preferential magnetic flux penetration into the material can be seen in (c) and (d), indicated by red arrows; the direction of which is at an angle different from the direction of the favored dislocation (blue-green line).

In order to further investigate the correlation between flux penetration and the microstructural defects (in this case dislocations), the flux penetration area was analyzed using electron backscatter diffraction (EBSD). By calculating the orientation difference of one local area with respect to areas surrounding it, a local average misorientation (LAM) map was generated from EBSD data. Figure 11 shows the LAM map of the flux penetration area on the sample surface, where about 2 to 3 degrees of misorientations (green contrast) were noticed. This is believed to be caused by a higher density of geometrically necessary dislocations in this area.

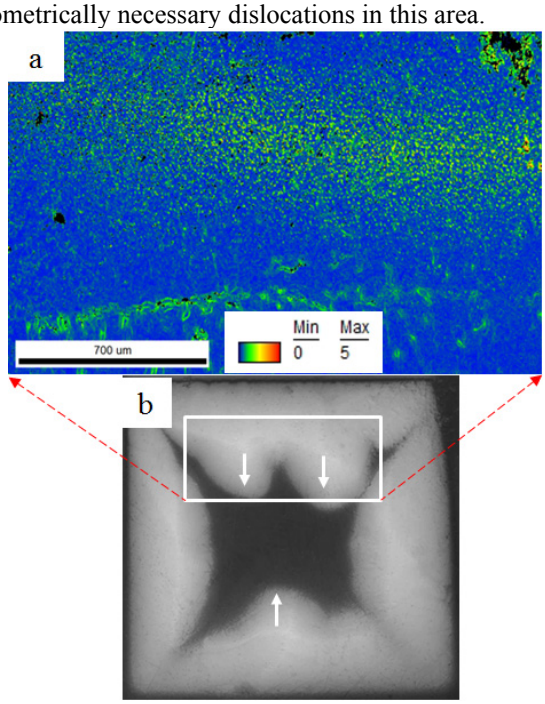

Figure 11: Local average misorientation map (a) of (b) the magneto-optical flux penetration (white arrows) area at T = 8.2K and zero magnetic field (reduced from H = 52mT).

EBSD analyses above provide the evidence of the correlation between magnetic flux penetration and dislocations in niobium; however, the reason for the observed flux penetration directions with respect to the slip plane and direction is still an open question.

CONCLUSION

In this work, dislocations were strategically introduced into single crystal niobium samples by deformation, which were then characterized under a MO imaging microscope to observe the magnetic flux behavior due to the introduced dislocations. EBSD-OIM analysis shows a higher density of geometrically necessary dislocations in the magnetic flux penetration area, providing a correlation between preferential flux penetration and dislocations for the first time. Future experiments will be aimed at clarifying the reasons behind this correlation.

REFERENCES

[1] Singer, W., "SRF Cavity Fabrication and Materials", arXiv preprint arXiv:1501.07142, 2015.

[2] Bieler, T.R., et al., "Physical and mechanical metallurgy of high purity Nb for accelerator cavities", Physical Review Special Topics - Accelerators and Beams, 2010. **13**(3): p. 031002.

[3] Saito, K., "State-of-the-Art and Future Prospects in RF Superconductivity", Proceedings of IPAC2012, New Orleans, Louisiana, USA.

[4] Ciovati, G. and A. Gurevich, "Evidence of high-field radio-frequency hot spots due to trapped vortices in niobium cavities", Physical Review Special Topics - Accelerators and Beams, 2008. **11**(12): p. 122001.

[5] Matsushita, T., "Flux pinning in superconductors", Vol. 164. 2007, New York: Springer.

[6] Polyanskii, A., et al. "Magneto-Optical Study High-Purity Niobium for Superconducting RF Application", in AIP Conference Proceedings-American Institute of Physics. 2011.

[7] Hull, D. and D.J. Bacon, "Introduction to dislocations", Vol. 257. 1984: Pergamon Press Oxford.

[8] Baars, D., Investigation of active slip systems in high purity single crystal niobium", 2013, Michigan State University.

[9] Polyanskii, A., D. Feldmann, and D. Larbalestier, "Magneto-optical characterization techniques", The Handbook on Superconducting Materials," Edited by David Cardwell and David Ginley, Institute of Physics UK, 2003. **1551**.

[10] Schatz, P. and A. McCaffery, "The faraday effect", Quarterly Reviews, Chemical Society, 1969. **23**(4): p. 552-584.

[11] "UiO: Department of Physics website", Available from: http://www.mn.uio.no/fysikk/english/research/groups/amks/superconductivity/mo/